J. Fluid Mech. (2007), *vol.* 580, *pp.* 145–168. © 2007 Cambridge University Press
doi:10.1017/S0022112007005344 Printed in the United Kingdom

A wave propagation model of blood flow in large vessels using an approximate velocity profile function

DAVID BESSEMS, MARCEL RUTTEN AND FRANS VAN DE VOSSE

Department of Biomedical Engineering, Eindhoven University of Technology, Postbus 513, 5600 MB Eindhoven, The Netherlands

(Received 1 February 2005 and in revised form 17 October 2006)

Lumped-parameter models (zero-dimensional) and wave-propagation models (one-dimensional) for pressure and flow in large vessels, as well as fully three-dimensional fluid–structure interaction models for pressure and velocity, can contribute valuably to answering physiological and patho-physiological questions that arise in the diagnostics and treatment of cardiovascular diseases. Lumped-parameter models are of importance mainly for the modelling of the complete cardiovascular system but provide little detail on local pressure and flow wave phenomena. Fully three-dimensional fluid–structure interaction models consume a large amount of computer time and must be provided with suitable boundary conditions that are often not known. One-dimensional wave-propagation models in the frequency and time domain are well suited to obtaining clinically relevant information on local pressure and flow waves travelling through the arterial system. They can also be used to provide boundary conditions for fully three-dimensional models, provided that they are defined in, or transferred to, the time domain.

Most of the one-dimensional wave propagation models in the time domain described in the literature assume velocity profiles and therefore frictional forces to be in phase with the flow, whereas from exact solutions in the frequency domain a phase difference between the flow and the wall shear stress is known to exist. In this study an approximate velocity profile function more suitable for one-dimensional wave propagation is introduced and evaluated. It will be shown that this profile function provides first-order approximations for the wall shear stress and the nonlinear term in the momentum equation, as a function of local flow and pressure gradient in the time domain. The convective term as well as the approximate friction term are compared to their counterparts obtained from Womersley profiles and show good agreement in the complete range of the Womersley parameter α. In the limiting cases, for Womersley parameters $\alpha \to 0$ and $\alpha \to \infty$, they completely coincide. It is shown that in one-dimensional wave propagation, the friction term based on the newly introduced approximate profile function is important when considering pressure and flow wave propagation in intermediate-sized vessels.

1. Introduction

The propagation of pressure and flow waves in the arterial system and especially its influence on the development of stenotic regions, aneurysms and other vascular diseases has been the subject of many studies (Anliker, Rockwell & Ogden 1971;

Hughes & Lubliner 1973; Young & Tsai 1973; Stergiopulos, Westerhof & Westerhof 1999; Olufsen & Peskin 2000; Lagrée 2000; Formaggia *et al.* 2001; Wan *et al.* 2002; Sherwin *et al.* 2003; Wang & Parker 2004). Haemodynamic factors such as blood pressure and flow have received much attention as intraluminal pressure is found to regulate the arterial wall thickness through its effects on wall tension (Fung 1993), whereas blood flow regulates the lumen diameter through changes in wall shear stress (Fung 1993). To obtain detailed information on these crucial parameters in the development of atherosclerosis, much effort has been put into the development and validation of computational methods for fully three-dimensional analysis of time-dependent flow in distensible artery segments (see e.g. Taylor, Hughes & Zarins 1998; Gijsen, van de Vosse & Janssen 1999*a*,*b*; van de Vosse *et al.* 2003). Using these methods, detailed velocity fields and pressure gradients can be obtained within the region of interest. As a result of the large amount of computer resources associated with these computations, however, most three-dimensional computational methods can only be applied to a small segment of the arterial system and hence appropriate assumptions on the proximal and distal part of the arterial tree must be provided. Suitable boundary conditions can be obtained by using appropriate simplified models of the total cardiovascular system, such as zero-dimensional lumped-parameter models (de Pater & van den Berg 1964; Westerhof *et al.* 1969) and one-dimensional wave-propagation models in the frequency domain (Womersley 1957; Cox 1968, 1970) and time domain (Tsou *et al.* 1971; Hughes & Lubliner 1973; Stergiopulos *et al.* 1999; Olufsen & Peskin 2000; Formaggia *et al.* 2001; Wan *et al.* 2002; Sherwin *et al.* 2003; Wang & Parker 2004).

Some important phenomena of wave propagation are difficult to describe with lumped-parameter models, whereas the nonlinear characteristics of the governing equations and the constitutive equations that describe the mechanical properties of the arterial wall cannot always be described in the frequency domain. Moreover, as three-dimensional patient-specific computational models are generally defined in the time domain, time-domain-based one-dimensional models are preferable in the provision of boundary conditions. They have been shown to be a simple tool in describing the propagation of the pressure and flow waves travelling through the arterial system or through a segment of this system. When dealing with one-dimensional wave propagation formulations, assumptions need to be made on local velocity profiles in order to obtain proper estimates for the nonlinear and friction term in the momentum equation integrated over the local cross-sectional area. The above papers assume either a Poiseuille profile (Stergiopulos *et al.* 1999; Wan *et al.* 2002; Wang & Parker 2004) or the velocity profile to be some other function of the local flow (Hughes & Lubliner 1973; Olufsen & Peskin 2000; Formaggia *et al.* 2001; Sherwin *et al.* 2003), both resulting in friction forces in phase with the flow. When interest is in the attenuation of the pressure wave and in the wall shear stress, however, these assumptions are insufficient, as from a fluid dynamical point of view a phase difference between the wall shear stress and the local flow may occur as a result of a time-dependent phase difference between the velocity in the central core of the vessel and the velocity near the vessel wall.

In this paper an approximate velocity profile function will be introduced, providing proper estimates for the nonlinear and friction terms. In § 2, a mathematical formulation of the one-dimensional wave propagation theory for flow in large vessels according to Hughes & Lubliner (1973) will briefly be described. Then this theory will be extended by introducing a velocity profile function that depends on the Womersley parameter α, the local flow rate and the pressure gradient. This model

is different from the model proposed by Olufsen (1999) where a linear boundary layer profile was introduced, again not allowing for a phase difference between the boundary layer flow and the flow in the inviscid core of the vessel. The model is also different from the approach of Tsou *et al.* (1971) where the velocity profile is represented by a third-degree polynomial expansion where the coefficients depend on time and axial position. In that case an extra equation has to be solved to obtain the coefficients of the expansion and no distinction between the viscous layer and the inviscid core can be made. In the work of Zagzoule, Khalid-Naciri & Mauss (1991) an asymptotic expression, relating the wall shear stress to the instantaneous flow, was deduced. The use of this expression in one-dimensional wave propagation, however, restricts the model to low-Womersley-number regions ($\alpha < 6$) so it cannot be used in the total physiological range of α. Lagrée (2000) closes the system of one-dimensional equations by defining a set of coefficients dependent solely on α, derived from Womersley's theory and based on the fundamental mode of the flow pulse. The resulting wall shear stress and nonlinear term for single harmonic flow pulses closely approximate their analytical counterparts based on the Womersley theory. For multiharmonic flow pulses at high values of α, however, we will show that the closure used by Lagrée no longer provides accurate estimates for the wall shear stress and the nonlinear term, even for the case where the Womersley solution should be retained.

In this study approximate profiles are derived by assuming inertia-dominated flow in the central core of the tube and friction-dominated flow near the vessel wall. Solutions in these areas are coupled using cross-sectional mass conservation, allowing for profiles different from Womersley profiles based on a single harmonic. This approach allows the possibility of extending the method to constitutive models for which no analytical solution is available and non-harmonic input, provided that a reasonable distinction between the central core and the viscous layer can be modelled.

In § 3, the friction term obtained from the theory proposed in this study is compared to the one presented in Young & Tsai (1973) based on Womersley's solution in the frequency domain (Womersley 1957). The nonlinear term is compared to the one obtained directly from velocity profiles derived from Womersley's theory. Finally, the effect of the friction term on wave propagation is illustrated by comparing the pressure gradient and flow resulting from wave propagation using our velocity profile approximation with wave propagation using Poiseuille friction, in a physiological range.

2. Theory

2.1. *Conservation of mass and momentum in one dimension*

The derivation of the governing equations for one-dimensional wave propagation in incompressible fluids, including outflow due to branching, is taken from Hughes & Lubliner (1973). Based on the Reynolds transport theorem, the differential equations for conservation of mass and momentum balance are derived for a geometry such as depicted in figure 1. The integrated continuity equation in area–velocity $(A, \overline{v}_z)$-formulation is written as

$$\frac{\partial A}{\partial t} + \frac{\partial}{\partial z}(A\overline{v_z}) + \Psi = 0, \tag{2.1}$$

with t being the time, z the axial coordinate, A the local cross-sectional area and Ψ the volumetric outflow per unit length. The fluid velocity $\boldsymbol{v} = (v_x, v_y, v_z)$ in the axial direction is denoted by v_z and an overbar indicates the cross-sectional mean.

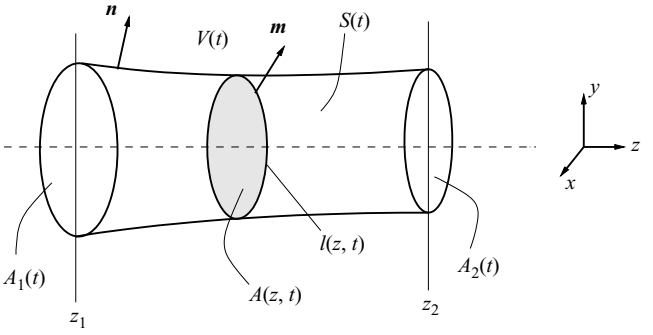

FIGURE 1. The geometry of part of a vessel along the z-axis, bound by cross-sectional surfaces $A_1(z=z_1)$ and $A_2(z=z_2)$ and circumferential surface S. The total volume is denoted by the symbol V, an arbitrary cross-section perpendicular to the z-axis by A and its boundary by l.

The physiologically more relevant pressure–flow (p, q)-formulation can be obtained by introducing a constitutive relation expressing the response of the vessel wall to pressure variations. For reasons of simplicity, here an $A = A(p(t))$ relation is chosen according to

$$\frac{\partial A}{\partial t} = \frac{\partial A}{\partial p}\frac{\partial p}{\partial t} \equiv C\frac{\partial p}{\partial t}, \tag{2.2}$$

but more complicated and visco-elastic properties can also be modelled. Here $C(z, t)$ is the compliance of the vessel, which can be obtained either from experimental data or from a constitutive model of the arterial wall. A more detailed description of the constitutive model used in this work is presented in § 3. After introducing volume flow $q \equiv A\overline{v}_z$, the following (p, q)-formulation can be derived:

$$C\frac{\partial p}{\partial t} + \frac{\partial q}{\partial z} + \Psi = 0. \tag{2.3}$$

When assuming a no-slip condition for the local velocity profile, the momentum balance from Hughes & Lubliner (1973) can be written as

$$\frac{\partial q}{\partial t} + \frac{\partial A\overline{v_z^2}}{\partial z} + \frac{A}{\rho}\frac{\partial p}{\partial z} = Af_z + \oint_l \left(\frac{\eta}{\rho}\frac{\partial v_z}{\partial m}\right)\mathrm{d}l + A\frac{\eta}{\rho}\overline{\frac{\partial^2 v_z}{\partial z^2}}. \tag{2.4}$$

Here, f_z are the body forces acting on the fluid in axial direction and $\boldsymbol{m} = (m_x, m_y, 0)$ is the outward normal to l. The fluid density and viscosity are referred to as ρ and η respectively. The last term on the right of (2.4) is obtained by retaining the diffusion forces in the derivation from Hughes & Lubliner (1973). We choose to keep this term for reasons of numerical stability. Equation (2.4) is the one-dimensional momentum balance in an (A, q)-formulation. For a more thorough derivation of the above equations, see Hughes & Lubliner (1973). On using the approximation

$$\oint_l \frac{\eta}{\rho}\frac{\partial v_z}{\partial m}\mathrm{d}l \approx \frac{2\pi a}{\rho}\tau_w \tag{2.5}$$

with τ_w as the wall shear stress, and the definition

$$\gamma \equiv A\overline{v_z^2} = \int_A v_z^2 \mathrm{d}A, \tag{2.6}$$

equation (2.4) becomes

$$\frac{\partial q}{\partial t} + \frac{\partial \gamma}{\partial z} + \frac{A}{\rho}\frac{\partial p}{\partial z} = Af_z + \frac{2\pi a}{\rho}\tau_w + \frac{\eta}{\rho}\frac{\partial^2 q}{\partial z^2}, \tag{2.7}$$

where the last term on the right-hand side has been derived using the Leibniz' theorem in combination with boundary conditions $v_z|_{r=a} = 0$ and $\partial v_z/\partial z|_{r=0} = 0$. Note that (2.5) is exact for circular cross-sections A but can be generalized for non-circular cross-sections using $a = \sqrt{A/\pi}$. The term γ will be referred to as the (nonlinear) convection term. To solve (2.7) with respect to the pressure p and the flow q in combination with the one-dimensional mass conservation equation (2.2) and a constitutive relation between p and A, more information about the local velocity profile v_z is needed to provide proper estimates for the convection term γ (2.6) and the wall shear stress τ_w (2.5), expressed in terms of p and q. Note that, for this, we do not need an exact description of the velocity profile as long as we have good approximations for the integral of its square and its derivative at the wall. Whereas previous work in the time domain used mainly flat or Poiseuille profiles, in this paper an alternative profile function will be derived to approximate the above terms, presented next.

2.2. *An approximate velocity profile function*

Here a relation for $\boldsymbol{v}(\boldsymbol{x}, t)$ expressed in terms of $p(z, t)$ and $q(z, t)$ is derived to provide proper estimates for the convection term γ and the friction term τ_w. Hughes & Lubliner (1973) provide following expression:

$$\boldsymbol{v}_A = \boldsymbol{0} \quad \text{and} \quad v_z(\boldsymbol{x}_A, t) = \phi(x, y)\overline{v}_z(z, t) \tag{2.8}$$

with ϕ such that the axial velocity at the wall is zero (and so $\phi|_l = 0$) and the mean cross-sectional velocity equals $\overline{v}_z(z, t)$. This formulation implies that in all cases the shape of the profile is both constant over time and constant along the axis of the vessel. From a mathematical point of view this is a convenient choice that will simplify the momentum equation (2.4) significantly. From a physical perspective, however, the choice presented in (2.8) is less obvious. As the velocity in the core of the vessel does not need to be in-phase with the velocity in the outer layer, a velocity profile that changes its shape in time must be chosen.

Here we consider the Navier–Stokes equations for fully developed flow in straight tubes driven by a given pressure gradient

$$\rho\frac{\partial v_z}{\partial t} = -\frac{\partial p}{\partial z} + \eta\frac{1}{r}\frac{\partial}{\partial r}\left(r\frac{\partial v_z}{\partial r}\right) \tag{2.9}$$

with $r = \sqrt{x^2 + y^2}$ as the radial coordinate. We will consider the situation as depicted on the left in figure 2. To obtain a good approximation of the solution of (2.9) close to the wall, we take the limit as r approaches a

$$\lim_{r\to a}\left(\rho\frac{\partial v_z}{\partial t}\right) = \lim_{r\to a}\left(-\frac{\partial p}{\partial z} + \eta\frac{1}{r}\frac{\partial}{\partial r}\left(r\frac{\partial v_z}{\partial r}\right)\right). \tag{2.10}$$

Owing to the no-slip condition at the wall, the left-hand side of (2.10) will be zero. As the pressure gradient is constant over the cross-sectional area, we have

$$0 = -\frac{\partial p}{\partial z} + \lim_{r\to a}\left(\eta\frac{1}{r}\frac{\partial}{\partial r}\left(r\frac{\partial v_z}{\partial r}\right)\right) \tag{2.11}$$

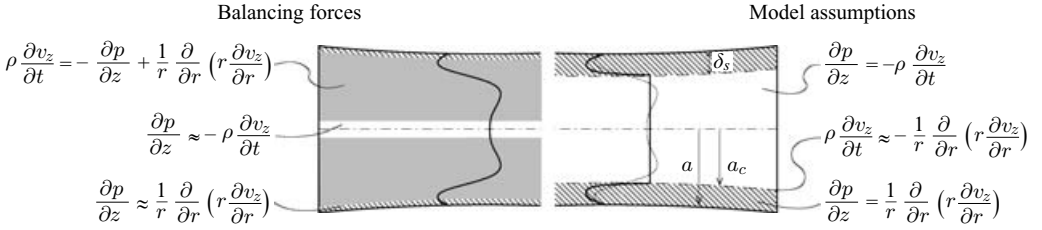

FIGURE 2. The geometry of part of a vessel with local radius a. The present fluid dynamical forces are shown on the left and on the right our approximation, where a_c is the core radius and $\delta_s = a - a_c$ the viscous layer. The solid curve on the left represents an exact velocity profile and the solid curve on the right the approximation according to our method.

close to the wall. In the central core viscous forces are assumed to be negligible, so

$$\rho\frac{\partial v_z}{\partial t} = -\frac{\partial p}{\partial z}, \tag{2.12}$$

which allows a flat profile in this region. In the region between these two limiting cases the grey area is defined (see figure 2) where all three terms should balance according to equation (2.9). In this area the velocity profile will be continuous and bounded both by the velocity near the wall and the velocity in the central core. Exact solutions of (2.9), providing exact velocity profiles, can only be derived in the frequency domain (Womersley 1957). As our only interest is in providing reasonable approximations for the nonlinear term $\gamma = \int v_z^2 \mathrm{d}A$ and the friction term $\partial v_z/\partial r|_{r=a}$ any other velocity profile doing so is admissible, as long as mass conservation $\int v_z \mathrm{d}A$ is satisfied. We chose to model the limiting case where the grey area of figure 2 becomes infinitesimally small, leaving only the inviscid area in the central core and the purely viscous layer near the vessel wall as depicted on the right in figure 2. At the transition between these two areas we connect the velocity v_z in the viscous layer to the velocity in the central core v_c, which is still unknown but can be eliminated (written in terms of q) using cross-sectional mass conservation. A first-order estimate of the thickness of the viscous layer δ_s for fully developed flow in straight rigid tubes is derived from the equilibrium between inertia forces $\rho\ \partial v_z/\partial t$ and viscous forces $\eta\ \partial^2 v_z/\partial r^2$ at the transition from the viscous layer to the inviscid core. This yields $\delta_s = O(\sqrt{\eta/\rho\omega}) = O(a/\alpha)$, with α being the Womersley parameter and ω representing the angular frequency. Consequently, the central core is related to the Womersley parameter according to

$$\frac{a_c}{a} = \max\left[0, \left(1 - \frac{k}{\alpha}\right)\right] \quad \text{with} \quad \alpha = a\sqrt{\frac{\rho\omega}{\eta}} \quad \text{and} \quad k = O(1), \tag{2.13}$$

where the exact value of k will be defined later in this section. For blood flow a rough estimation yields: $\eta/\rho \approx 6 \times 10^{-6}\,\mathrm{m^2\,s^{-1}}$ (Gijsen *et al.* 1999*a*) and $\omega = 2\pi/T \approx 6\ \mathrm{s^{-1}}$ resulting in $\delta_s \approx 1$ mm (specifically, $\delta_s \approx \min[a, 1\text{ mm}]$) for all arteries. To incorporate the above into the velocity profile function the governing equations in the viscous layer will be solved for the axisymmetric case. This shall be done using proper boundary conditions to connect the velocity profile in this layer to the velocity in the central core. In this central core (2.12) results in a flat profile according to.

$$v_z(r, z, t) = v_c(z, t) \quad \text{for } r < a_c, \tag{2.14}$$

where v_c is left undetermined. In the viscous layer, equilibrium between the pressure gradient and the friction forces is assumed according to (2.11):

$$0 = -\frac{\partial p}{\partial z} + \eta \frac{1}{r}\frac{\partial}{\partial r}\left(r\frac{\partial v_z}{\partial r}\right) \quad \text{for } a_c \leqslant r < a. \tag{2.15}$$

After integration of (2.15) with respect to the radius r twice, together with the boundary conditions $v_z|_{r=a_c} = v_c$ and $v_z|_{r=a} = 0$ the following profile is obtained:

$$v_z = -\frac{a^2}{4\eta}\frac{\partial p}{\partial z}(1-\xi^2) + \frac{\ln \xi}{\ln \xi_c}\left[v_c + \frac{a^2}{4\eta}\frac{\partial p}{\partial z}(1-\xi_c^2)\right] \quad \text{for } a_c \leqslant r < a, \tag{2.16}$$

with $\xi = r/a$ the dimensionless radius, and $\xi_c = a_c/a$ the dimensionless core diameter. Integration of (2.14) and (2.16) over the cross-sectional area A results in a relation between the core velocity $v_c(z,t)$ and the cross-sectional mean velocity $\overline{v}_z \equiv q/A$ dependent on the radius of the core a_c and the pressure gradient $\partial p/\partial z$, according to

$$v_c = \left[\frac{\ln \zeta_c}{\zeta_c - 1}\right]\overline{v}_z + \frac{a^2}{4\eta}\left[1 - \zeta_c + \frac{1}{2}(\zeta_c + 1)\ln \zeta_c\right]\frac{\partial p}{\partial z}, \tag{2.17}$$

with $\zeta_c = \xi_c^2$. Substitution of this relation in (2.16) yields an expression for the total velocity profile $v_z(\boldsymbol{x}, t)$:

$$v_z = \frac{-\ln \hat{\zeta}}{1-\zeta_c}\,\overline{v}_z - \frac{a^2}{4\eta}\left[1 - \hat{\zeta} + \tfrac{1}{2}(\zeta_c + 1)\ln \hat{\zeta}\right]\frac{\partial p}{\partial z}, \tag{2.18}$$

with

$$\zeta = \xi^2 \quad \text{and} \quad \hat{\zeta} = \max[\zeta,\ \zeta_c]. \tag{2.19}$$

The simple relation (2.8) of Hughes & Lubliner (1973) is now replaced by the more complex one

$$v_z(\boldsymbol{x}, t) = \phi_1(\zeta, \zeta_c)\,\overline{v}_z(z,t) - \phi_2(\zeta, \zeta_c)\frac{a^2}{4\eta}\frac{\partial p(z,t)}{\partial z} \tag{2.20}$$

with ϕ_1 and ϕ_2 defined by

$$\phi_1(\zeta, \zeta_c) = \frac{-\ln \hat{\zeta}}{1-\zeta_c} \quad \text{and} \quad \phi_2(\zeta, \zeta_c) = 1 - \hat{\zeta} + \tfrac{1}{2}(\zeta_c + 1)\ln \hat{\zeta}. \tag{2.21}$$

Note that, in cylindrical coordinates

$$\int_0^1 \phi_1 \xi \,\mathrm{d}\xi = \tfrac{1}{2} \quad \text{and} \quad \int_0^1 \phi_2 \xi \,\mathrm{d}\xi = 0 \tag{2.22}$$

and, consequently, the mean velocity does not depend on the second term on the right-hand side of (2.20). For the axisymmetric case the wall shear stress τ_w can be computed as

$$\tau_w\left(\frac{\partial p}{\partial z}, q, A, \xi_c\right) = \eta \frac{\partial v_z}{\partial r}\Big|_{r=a} = -\frac{2\eta}{(1-\zeta_c)a}\frac{q}{A} + \frac{a}{4}(1-\zeta_c)\frac{\partial p}{\partial z}. \tag{2.23}$$

A detailed derivation of the nonlinear term $\gamma = A\overline{v^2}_z$ is presented in Appendix A, leading to the expression

$$\gamma\left(\frac{\partial p}{\partial z}, q, A, \xi_c\right) = \delta_1 \frac{q^2}{A} + \delta_2 q \frac{a^2}{4\eta}\frac{\partial p}{\partial z} + \delta_3 A\left(\frac{a^2}{4\eta}\frac{\partial p}{\partial z}\right)^2, \tag{2.24}$$

where δ_1, δ_2 and δ_3 are functions dependent solely on the dimensionless core thickness ζ_c according to

$$\left.\begin{aligned}\delta_1(\zeta_c) &= \int_0^1 \phi_1^2 \,\mathrm{d}\zeta = \frac{2-2\zeta_c(1-\ln\zeta_c)}{(1-\zeta_c)^2}\\ \delta_2(\zeta_c) &= -2\int_0^1 \phi_1\phi_2 \,\mathrm{d}\zeta = \frac{1+4\zeta_c(1+\ln\zeta_c)-\zeta_c^2(5-2\ln\zeta_c)}{1-\zeta_c}\\ \delta_3(\zeta_c) &= \int_0^1 \phi_2^2 \,\mathrm{d}\zeta = \tfrac{1}{3}+\zeta_c(3+2\ln\zeta_c)-\zeta_c^2(3-2\ln\zeta_c)-\tfrac{1}{3}\zeta_c^3.\end{aligned}\right\} \tag{2.25}$$

The resulting velocity profiles, corresponding wall shear stresses and nonlinear forces at different Womersley numbers α will be compared to Womersley's theory in a later section.

2.3. *Viscous layer thickness*

The only parameter yet to be determined in order for the velocity profile function (and thus the wall shear stresses and nonlinear forces) to be known, is the viscous layer thickness. A physically relevant value for this parameter must be provided as a function of the local geometry and the local fluid dynamical parameters. For friction-dominated flow ($\alpha < k$) Poiseuille friction can be recovered by substitution of

$$\frac{\partial p}{\partial z} = -Rq = \frac{-8\eta}{\pi a^4} q \tag{2.26}$$

into equation (2.23) and setting $\zeta_c = 0$. For inertia-dominated flow ($\alpha \gg 1$) (2.13) gives

$$1-\zeta_c = 1-\xi_c^2 \approx \frac{2k}{\alpha}. \tag{2.27}$$

Moreover,

$$\frac{\partial q}{\partial t} \approx -\frac{A}{\rho}\frac{\partial p}{\partial z} \tag{2.28}$$

or, on introducing the harmonic solutions $q = \hat{q}\,\mathrm{e}^{\mathrm{i}\omega t}$ and $p = \hat{p}\,\mathrm{e}^{\mathrm{i}\omega t}$,

$$\hat{q} \approx \frac{\mathrm{i}A}{\rho\omega}\frac{\partial \hat{p}}{\partial z}, \tag{2.29}$$

with $\hat{p}$ and $\hat{q}$ respectively the complex amplitude of p and q for each harmonic of the pressure. In this case, by substitution of (2.29), (2.27) and (2.13) into (2.23), the corresponding complex amplitude of the wall shear stress $\hat{\tau}_w$ becomes

$$\hat{\tau}_w = \frac{1}{\alpha}\left(k - i\frac{2}{k}\right)\hat{\tau}_w^p, \tag{2.30}$$

with τ_w^p equal to the Poiseuille wall shear stress. As our main interest is in providing the proper wall shear stress, (2.30) is compared to Womersley's theory and for $k = \sqrt{2}$ they are fully equivalent. Consequently, for relatively cylindrical parts of the vessel (i.e. for $\partial A/\partial z \ll a$) and sufficiently far from geometrical discontinuities, the following approximation for ξ_c can be used:

$$\xi_c = \max[0,\ 1-\sqrt{2}/\alpha]. \tag{2.31}$$

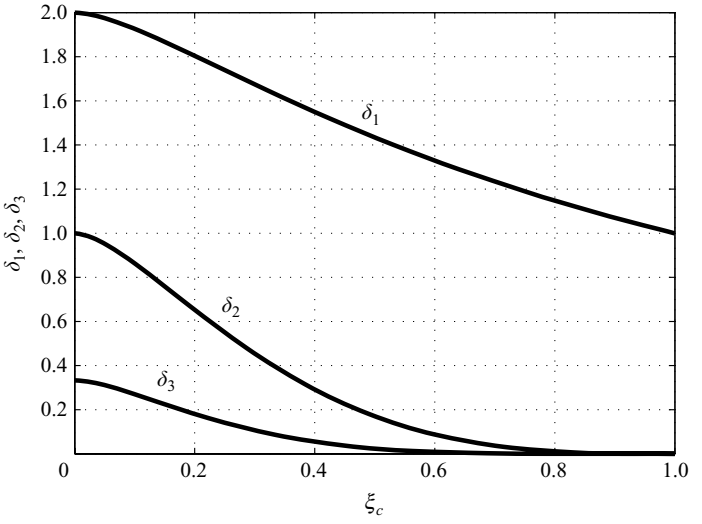

FIGURE 3. Parameters δ_1, δ_2, and δ_3 as a function of the dimensionless core radius ξ_c.

2.4. *Wave propagation*

In addition to the $(1+\delta)q^2/A$ term in the original equation of Hughes & Lubliner (1973) extra nonlinear terms now appear in $\gamma(p,q)$, given in (2.24). Since the multiplication factors corresponding to δ_i are of the same order of magnitude, the importance of the terms on the right-hand side of equation (2.24) depends on the magnitude of the functions δ_1, δ_2 and δ_3. These are plotted against the dimensionless core radius ξ_c in figure 3. The case of a Poiseuille flow, where $\zeta_c \to 0$ and $\partial p/\partial z = -(8\eta/a^2)\bar{v}_z$, yields $1+\delta = \delta_1 - \delta_2 + \delta_3 = 4/3$. For a flat profile, $\zeta_c \to 1$, which results in $1+\delta = \delta_1 = 1$, so both limiting cases are in complete correspondence with the original method. Since the influence of the nonlinear term is important mainly for large arteries at high Womersley numbers ($\alpha \gg 1$ and so $\xi_c \to 1$), in the remainder of this work the contributions of δ_2 and δ_3 will be neglected (see figure 3), resulting in a nonlinear term similar to the ones presented in the literature, e.g. Hughes & Lubliner (1973). The set of equations that follows from mass conservation, the momentum balance and a constitutive law for the wall material, together with the profile function and the wall shear stress, is

$$\left.\begin{aligned} &\frac{\partial A}{\partial t} + \frac{\partial q}{\partial z} = -\Psi, \\ &\frac{\partial q}{\partial t} + \frac{\partial}{\partial z}\left(\delta_1 \frac{q^2}{A}\right) + \frac{A}{\rho}\frac{\partial p}{\partial z} = A f_z + \frac{2\pi a}{\rho}\tau_w + \frac{\eta}{\rho}\frac{\partial^2 q}{\partial z^2}, \\ &p(z,t) = \tilde{p}(A(z,t); z, t), \end{aligned}\right\} \tag{2.32}$$

and

$$\left.\begin{aligned} v_z &= -\frac{\ln\hat{\zeta}}{1-\zeta_c}\frac{q}{A} - \frac{a^2}{4\eta}\left[1 - \hat{\zeta} + \tfrac{1}{2}(\zeta_c+1)\ln\hat{\zeta}\right]\frac{\partial p}{\partial z}, \\ \tau_w &= -\frac{2\eta}{(1-\zeta_c)a}\frac{q}{A} + \frac{a}{4}(1-\zeta_c)\frac{\partial p}{\partial z}, \end{aligned}\right\} \tag{2.33}$$

with γ, τ_w, $\hat{\xi}$ and ζ_c from (2.24), (2.23), and (2.19) respectively. The constitutive law expresses a relation between the local instantaneous pressure $p(z,t)$ and the local instantaneous cross-sectional area $A(z,t)$ for which a linear approach will be proposed in the next section.

For a comparison with results from Young & Tsai (1973) later on, the friction term in (2.33) will now be revised into a comparable format. Introducing the coefficients c_p and c_q as

$$c_p = 1 + \tfrac{1}{2}(1-\zeta_c), \qquad c_q = \tfrac{1}{2}(1-\zeta_c)^{-1}, \tag{2.34}$$

yields

$$\tau_w = -\frac{a}{2}\left[c_q R q - (c_p - 1)\frac{\partial p}{\partial z}\right] \tag{2.35}$$

for the wall shear stress with the resistance R per unit of length defined according to

$$R = \frac{8\eta}{\pi a^4}. \tag{2.36}$$

Using equation (2.13) with $k = \sqrt{2}$ gives

$$c_q = \frac{\alpha}{4k}\left(1 - \frac{\sqrt{2}}{2\alpha}\right)^{-1}, \qquad c_p = 1 + \frac{\sqrt{2}}{\alpha}\left(1 - \frac{\sqrt{2}}{2\alpha}\right) \quad \text{for } \alpha > \sqrt{2}. \tag{2.37}$$

Remark. For shear dominated flow in small arteries (quasi-static Poiseuille flow) a similar derivation gives $c_p + c_q = 2$ and since this is also the case for $\alpha = \sqrt{2}$, use of (2.37) gives

$$c_q = \frac{1}{2}, \qquad c_p = \frac{3}{2} \quad \text{for } \alpha \leqslant \sqrt{2}. \tag{2.38}$$

Substitution of (2.35) into the momentum equation of (2.32) without external forces and neglecting the nonlinear and diffusion terms gives

$$\frac{\partial p}{\partial z} = -\left[\frac{c_q}{2 - c_p}\right] R q - \left[\frac{1}{2 - c_p}\right] L_0 \frac{\partial q}{\partial t} \tag{2.39}$$

with $L_0 = \rho / A_0$ [kg m^{-5}] the inertance per unit of length.

2.5. *General set of equations*

To simplify the resulting set of equations for the general case a (p,q)-formulation with the pressure and the flow as parameters is proposed as this may be the best option with respect to linearization in $A(z,t)$. The cross-sectional area can be derived from the pressure using the linearized constitutive relation:

$$A(z,t) = \tilde{A}(p(z,t),z) = A_0(z) + C_0(p - p_0) \tag{2.40}$$

with the compliance per unit length C_0, based on thin-walled-cylinder theory for a linear elastic material, defined as

$$C_0 = \left.\frac{\partial A}{\partial p}\right|_{p=p_0} = \frac{2\pi(1-\mu^2)a_0^3}{hE}. \tag{2.41}$$

Here, μ is Poisson's ratio, E is Young's modulus and a_0 is the vessel radius at $p = p_0$. Using the p, q-formulation yields

$$\frac{\partial}{\partial t}\begin{bmatrix} p \\ q \end{bmatrix} + \boldsymbol{N}\frac{\partial}{\partial z}\begin{bmatrix} p \\ q \end{bmatrix} - \boldsymbol{D}\frac{\partial^2}{\partial z^2}\begin{bmatrix} p \\ q \end{bmatrix} + \boldsymbol{H}\begin{bmatrix} p \\ q \end{bmatrix} = \boldsymbol{f} \tag{2.42}$$

with

$$\boldsymbol{N} = \begin{bmatrix} 0 & C_0^{-1} \\ (2-c_p)\dfrac{A}{\rho} - \delta_1 \dfrac{q^2}{A^2} C_0 & \delta_1 \dfrac{2q}{A} \end{bmatrix}, \quad \boldsymbol{D} = \begin{bmatrix} 0 & 0 \\ 0 & \dfrac{\eta}{\rho} \end{bmatrix}, \tag{2.43}$$

$$\boldsymbol{H} = \begin{bmatrix} 0 & 0 \\ 0 & c_q \dfrac{A}{\rho} R + \dfrac{q}{A}\left(\dfrac{\partial \delta_1}{\partial z} - \dfrac{\delta_1}{A}\dfrac{\partial A}{\partial z}\right) \end{bmatrix}, \quad \boldsymbol{f} = \begin{bmatrix} -\Psi C_0^{-1} \\ A f_z \end{bmatrix} \tag{2.44}$$

and in terms of the original theory by Hughes & Lubliner (1973) (see Wan *et al.* 2002):

Wan *et al.* (2002)	this study
$\delta_1 = 1 + \delta = \dfrac{2+n}{1+n}$	$\delta_1 = \dfrac{2 - 2\zeta_c(1 - \ln \zeta_c)}{(1-\zeta_c)^2}$
$c_p = 1$	$c_p = 1 + \frac{1}{2}(1 - \zeta_c)$
$c_q = -\dfrac{N\rho}{RA^2} = \dfrac{n+2}{4}$	$c_q = \frac{1}{2}(1-\zeta_c)^{-1}$
with $N = -2(n+2)\pi\nu$	with $\zeta_c = \left(\dfrac{a_c}{a}\right)^2 \approx \left(1 - \dfrac{k}{\alpha}\right)^2$
where n is a free parameter	

(2.45)

Note that, in (2.42) for stability reasons, the term $(\eta/\rho)(\partial^2 q)/(\partial z^2)$ is kept, although it is small compared to the friction term $(2\pi\tau_w a)/\rho$.

2.6. *Computational method*

To analyse wave propagation using the approximate velocity profile function, a spectral element method is employed to solve the above sets of equations by discretization of the spatial domain using sixth-order one-dimensional spectral elements. A Galerkin weighted-residuals method is used to transform the set of partial differential equations into a spectral element space. This transformation is presented in Appendix B. The time derivatives are treated using a second-order backward differencing scheme and at each time step $\Delta t = 0.001$ [s] a Newton–Raphson iterative scheme is deployed to handle the nonlinear terms. This results in the following scheme:

$$\left[\tfrac{3}{2}\underline{M} + \Delta t \underline{S}_i^{n+1}\right]\boldsymbol{u}_{i+1}^{n+1} = 2\underline{M}\boldsymbol{u}^n - \tfrac{1}{2}\underline{M}\boldsymbol{u}^{n-1} + \Delta t \underline{M}\boldsymbol{f}_i^{n+1}, \tag{2.46}$$

where Δt is the time step used, $\boldsymbol{u} = [\underset{\sim}{u}_1 \;\; \underset{\sim}{u}_2]^T = [\underset{\sim}{p} \;\; \underset{\sim}{q}\,]^T$ and

$$\underline{S}_i^{n+1} = \underline{S}\left(\boldsymbol{u}_i^{n+1}\right), \qquad \underline{S}_0^{n+1} = \underline{S}(\boldsymbol{u}^n), \qquad \underline{S} = \underline{N} + \underline{D} + \underline{H}. \tag{2.47}$$

$\underline{M}$, $\underline{N}$, $\underline{D}$ and $\underline{H}$ are defined in (B 15). Furthermore,

$$\boldsymbol{f}_i^{n+1} = \boldsymbol{f}\left(\boldsymbol{u}_i^{n+1}\right), \qquad \boldsymbol{f}_0^{n+1} = \boldsymbol{f}(\boldsymbol{u}^n), \tag{2.48}$$

where $\boldsymbol{f} = [\underset{\sim}{f}_1 \;\; \underset{\sim}{f}_2]^T$. The method yields reliable and stable solutions without the use of any kind of upwinding or stabilization scheme. For a more detailed derivation of the final set of linear equations the reader is referred to Appendix B.

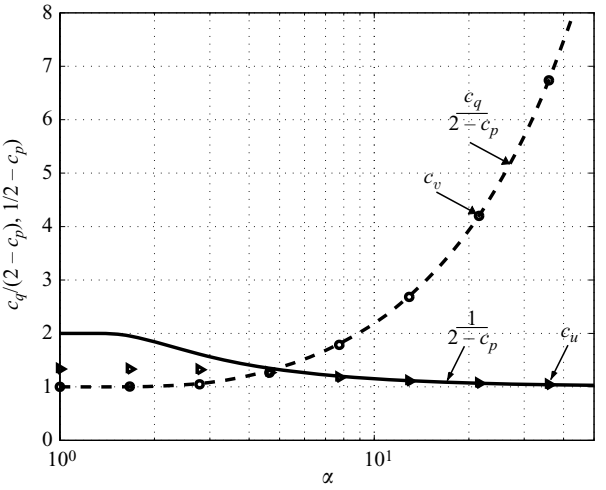

FIGURE 4. Coefficients $c_p/(2-c_p)$ and $1/(2-c_p)$ (dashed and solid lines respectively) as a function of α together with the values of c_v ($\circ$) and c_u ($\triangleright$) of Young & Tsai (1973).

3. Results

3.1. *Velocity profile function*

Using $k = \sqrt{2}$ as defined in the previous section, the approximations made for parameters c_p and c_q as defined by equations (2.37) and (2.38) can be evaluated and compared to results found in the literature. Young & Tsai (1973) gave an expression balancing the pressure gradient with the friction term and inertia forces, according to

$$\frac{\partial p}{\partial z} = -c_v\left(\frac{8\eta}{\pi a^4}\right)q - c_u\frac{\rho}{A}\frac{\partial q}{\partial t} \tag{3.1}$$

with coefficients c_v and c_u calculated from the exact solution as a function of the Womersley parameter α (Womersley 1957). In this work, equation (2.39) was obtained to compare coefficients $c_q/(2-c_p)$ and $1/(2-c_p)$ to the values of c_v and c_u from Young & Tsai respectively in a physiological range of α. Their values, when using equations (2.37) and (2.38) with $k = \sqrt{2}$ are plotted as solid lines in figure 4. For large values of α coefficients $c_q/(2-c_p)$ and $1/(2-c_p)$ are in good agreement with the values for c_u and c_v from Young & Tsai and for low values of α ($\alpha < k$) the combination of our coefficients as well as c_v and c_u correspond to Poiseuille friction since in this range the pressure gradient and the flow are directly related. Owing to the assumptions made when using the approximate velocity profile function, the intermediate values of α show some differences with respect to Womersley's theory.

The same observation can be made when comparing the nonlinear term $\gamma = \int v_z^2\,\mathrm{d}A$ derived from the approximate velocity profile function to γ derived from Womersley profiles. A single harmonic flow with radial frequency $\omega_q = 2\pi$ [s^{-1}] is prescribed and using values of the Womersley parameter in the range of $0 < \alpha \leqslant 16$ the corresponding pressure gradient $\partial p/\partial z$ is computed from Womersley's theory for flow in rigid tubes (Womersley 1957). Using this combination of q and $\partial p/\partial z$ the velocity profiles and the integral of their square root (γ) for both theories can be determined as a function of α and time t. It can easily be shown that for all α, $\gamma(t)$ is a single harmonic signal with radial frequency $\omega_\gamma = 2\omega_q$. This harmonic signal is

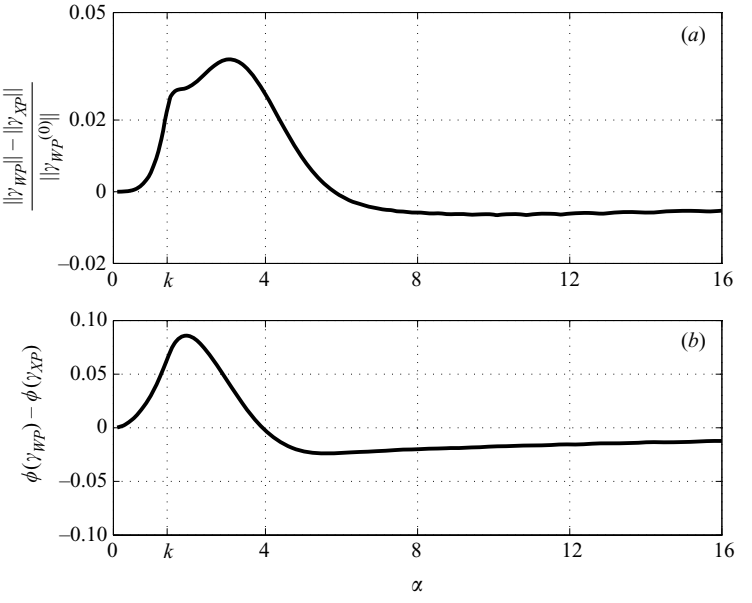

FIGURE 5. (*a*) Absolute difference between $\|\gamma_{WP}\|$ and $\|\gamma_{AP}\|$, normalized by $\|\gamma_{WP}(\alpha \to 0)\|$ as a function of α. (*b*) The phase difference between γ_{WP} and γ_{AP} as a function of α.

evaluated for both the approximate profiles (γ_{AP}) and the Womersley profiles (γ_{WP}) in the range of given α. Figure 5 shows the normalized (with $\gamma_{WP}(\alpha = 0)$) difference in the amplitude and the phase difference between both methods. Both the relative difference in amplitude and the phase difference approach 0 when α approaches 0. For large α, although more slowly, the differences also go to 0. Intermediate values of α show some differences in γ_{AP} and γ_{WP} as a result of the assumptions made when deriving the approximate velocity profile function.

The behaviour of τ_w and γ as a function of time is illustrated, along with the corresponding velocity profiles, for $\alpha = 0,\ 2,\ 4,\ 8,\ 16$ and ∞ in panels (*a*)–(*f*) of figure 6. Each panel represents a different Womersley number. The left-hand side of each panel shows the normalized flow and pressure gradient as function of the dimensionless time, followed (below) by the wall shear stress τ_w and nonlinear term γ from both methods. The illustration on the right-hand side of each panel shows the velocity profiles for both theories at 8 equidistant timesteps within one cycle. For low values of the Womersley parameter ($\alpha < \sqrt{2}$) the approximate velocity profile function exactly reproduces the expected Poiseuille profiles. For intermediate values of the Womersley parameter ($\alpha = 2,\ 4,\ 8,\ 16$) the profiles found using the approximate velocity profile method are more flat; however, an appropriate wall shear stress and convection parameter γ are found. Also, the phase shift between the pressure gradient and the wall shear stress as predicted by Womersley's theory is accurately described by the approximation. Note that in the case of a velocity profile proportional only to the flow, as in Hughes & Lubliner (1973) and Olufsen (1999), the wall shear stress would be in phase with the flow also. At higher values of the Womersley parameter ($\alpha \to \infty$) profiles are flat and well-predicted, resulting in good approximations for the wall shear stress and γ.

To demonstrate the possibility of determining τ_w and γ when imposing a physiological flow signal, multi-harmonic flow pulses from a coronary artery and

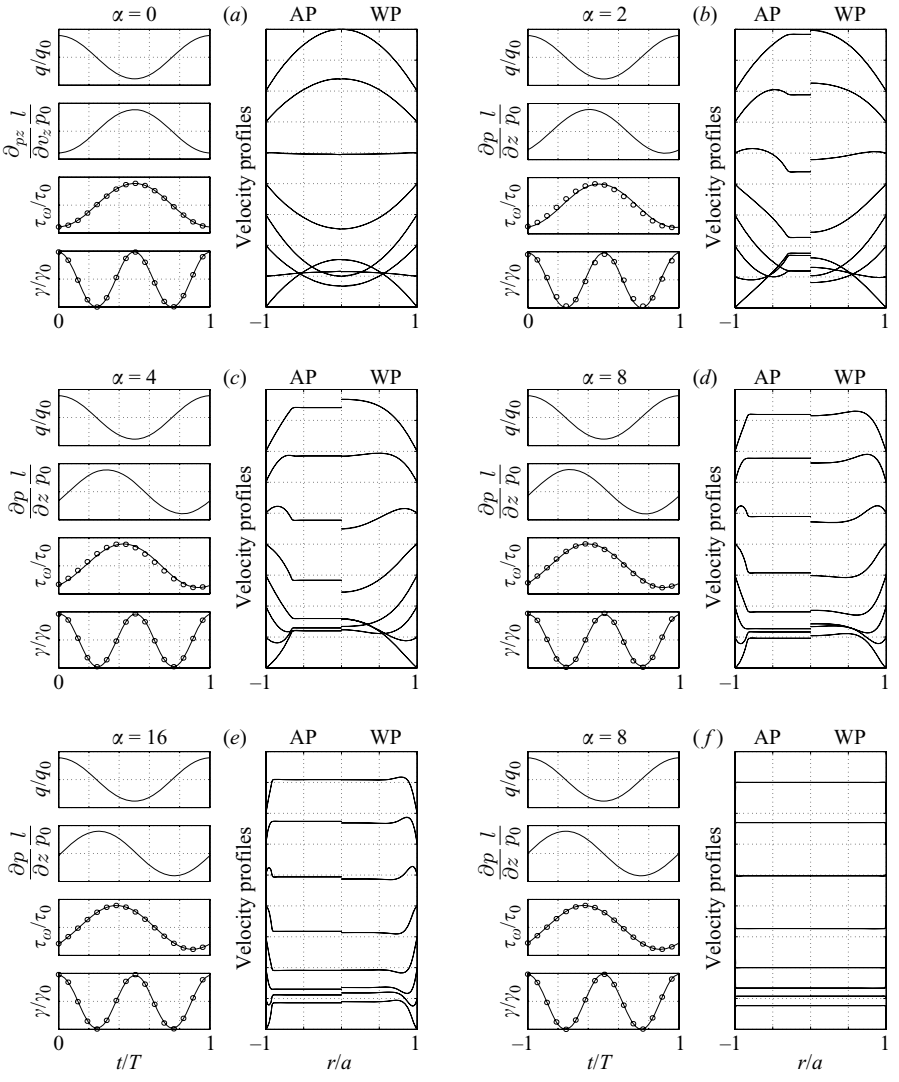

FIGURE 6. Each of the panels (*a*)–(*f*) represents velocity profiles $v_z(r,t)$ at 8 equidistant timesteps (right) for both our approximation (AP) and Womersley theory (WP) as a result of single-harmonic flow pulse q and pressure gradient $\partial p/\partial z$ (left-top), and resulting wall shear stress $\tau_w(t)$ and convection parameter $\gamma(t)$ from the approximate velocity profile function ($\circ$) and Womersley theory ($-$) (left-bottom) for $\alpha = 0,\ 2,\ 4,\ 8,\ 16$, and ∞.

the aorta (based on the first 10 harmonics of this signal) are used as an input for the previous computations. Figure 7 shows the result with $\alpha = 2$ for the left coronary artery and $\alpha = 12$ for the aorta. Although the estimations of α (and so δ_s) are based on the first harmonic of the flow signal, good approximations for the velocity profiles are obtained. The wall shear stress and the convection term resulting from the approximate velocity profiles also show good correspondence with Womersley's theory when imposing a multi-harmonic flow signal. Figure 7 also shows the resulting wall shear stress and nonlinear term according to the method by Lagrée (2000). Although his method is able to closely approximate the analytical wall shear stress

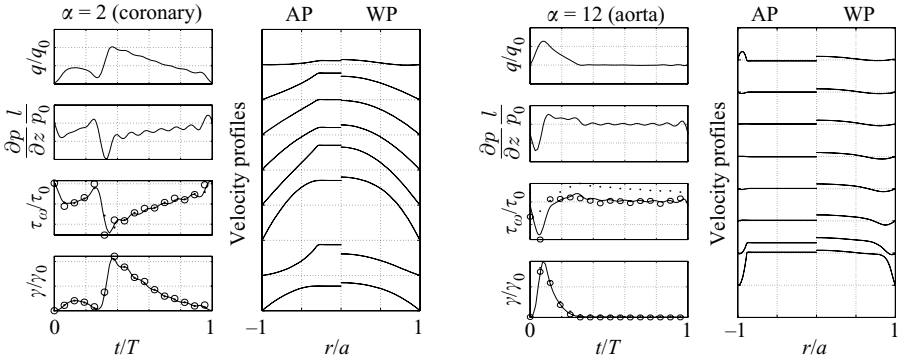

FIGURE 7. Panels (*a*) and (*b*) represent velocity profiles $v_z(r, t)$ at 8 equidistant timesteps (right) for both our approximation (AP) and Womersley theory (WP) as a result of multi-harmonic physiological flow pulse q and pressure gradient $\partial p/\partial z$ (left-top) obtained from the left coronary artery (*a*) and the aorta (*b*), and resulting wall shear stress $\tau_w(t)$ and convection parameter $\gamma(t)$ from Womersley theory (—), the approximate velocity profile function (○) and from the method by Lagrée (·) (left-bottom).

Vessel type	Length L [mm]	Local radius a_0 [mm]	Wall thickness h/a_0 [–]	Wave speed c_0 [m s^{-1}]	Windkessel parameters		
					R_1 [Ns m^{-5}]	R_2 [Ns m^{-5}]	C_T [m^5 N^{-1}]
Aorta	400	12.5–9.0	0.125	5.1	2.31×10^7	7.69×10^7	1.95×10^{-8}
FA	400	4.3–3.4	0.3	8.0	2.05×10^8	1.21×10^9	1.2×10^{-9}

TABLE 1. Data of vessels used for numerical experiments.

and nonlinear term at low values of α, figure 6(*b*) clearly demonstrates that at high values of α, when imposing a multi-harmonic flow signal, the wall shear stress no longer approaches its Womersley counterpart and certainly overestimates the wall shear stress in the diastolic phase where both q and $\partial p/\partial z$ approximate zero.

3.2. *Wave propagation*

The theory introduced in this study has already showed improvements over other assumed velocity profiles in approximating the wall shear stress and the convection term obtained by Womersley's theory. Whereas the new convection term yields only small changes in the one-dimensional equation (δ_2 and δ_3 are small with respect to δ_1), the expression for the friction term is significantly different from the friction term when assuming a Poiseuille profile. To determine whether the improved friction term influences the modelling of the waves travelling through the arterial system, a comparison in a physiological range is made between the friction term as defined by the velocity profile function and the friction defined by a Poiseuille profile (Hughes & Lubliner 1973). Using data from Olufsen & Peskin (2000), two compliant tubes are modelled both using six (sixth-order) spectral elements. One is an aorta-like vessel and the other is based on the femoral artery (FA) to include inertia-dominated flow ($\alpha \approx 12$) as well as flow where friction is more important ($\alpha \approx 4$). The geometric data (the radius a and the wall thickness h) of these vessels are given in table 1. Note that in our situation the aorta is modelled using less tapering than in Olufsen & Peskin

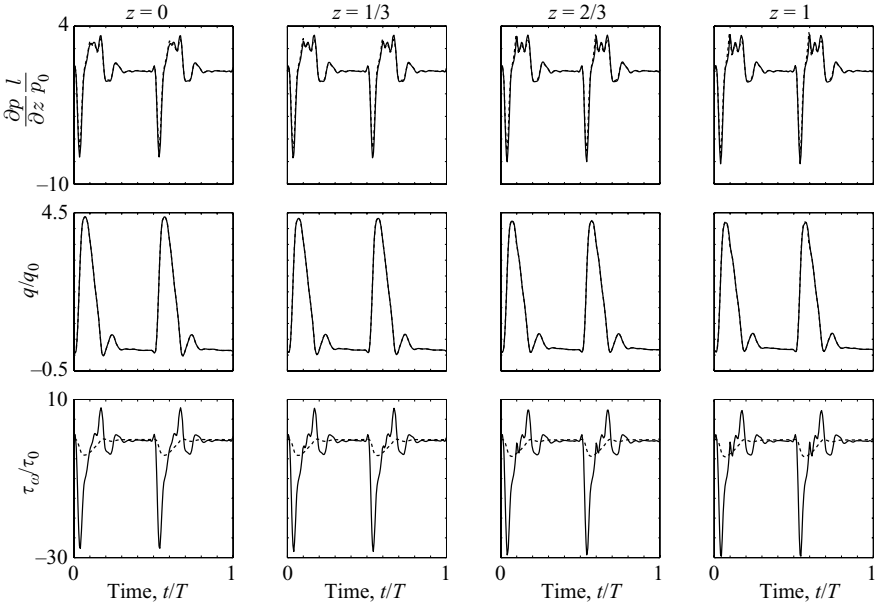

FIGURE 8. Analysis of the friction term in an aorta-like vessel, showing normalized pressure gradient $\partial p/\partial z$ (top), flow q (middle) and wall shear stress τ_w (bottom) as a function of time at four equidistant positions in the modelled vessel. Solid lines show results using our approximate velocity profile function whereas dashed lines show results using Poiseuille friction.

(2000) because in this work no side branches are modelled to subtract fluid from the vessel. The wall behaviour is assumed to be linear elastic according to (2.41) and the corresponding Young's modulus ($E = 4.0 \times 10^5$ [N m^{-1}]) and Poisson's ratio ($\nu = 0.3$ [–]) for both vessels are obtained from Westerhof *et al.* (1969). Blood properties are set at $\eta = 4.5 \times 10^{-3}$ [kg m^{-1} s] and $\rho = 1.04 \times 10^3$ [kg m^{-3}] for the viscosity and the density respectively, according to Porenta, Young & Rogge (1986). From the above data the constant wave speed c_0 for the two vessels, as given in table 1, is found using $c_0 = \sqrt{A_0/\rho\ C_0}$, where A_0 and C_0 are the cross-sectional area and the compliance at the initial pressure p_0 respectively. At the inlet of the aortic and the femoral tube flow pulses $q(z = 0, t)$ as measured by Olufsen & Peskin (2000) are prescribed as depicted in figure 8 and 9 respectively, whereas at the distal end of the vessels a three-element Windkessel is defined to relate the outlet pressure to the outlet flow (Stergiopulos, Young & Rogge 1992). Parameters R_1, R_2 and C_T are the corresponding terminal resistance, peripheral resistance and compliance respectively, as defined in table 1. The values of R_1 were obtained by modelling minimal reflections at the outlets according to

$$R_1 \sim Z_0 = \sqrt{\frac{L_0}{C_0}} = \sqrt{\frac{\rho\ h\ E}{2\pi^2(1-\nu^2)a_0^5}} \tag{3.2}$$

with $L_0 = \rho/A_0$ representing the local inertance, C_0 the local compliance as defined by (2.41) and Z_0 the local impedance at the distal end of the vessel. To obtain pressures in the physiological range, R_2 was derived using the total resistance R_T as

$$R_T = R_1 + R_2 = \overline{p}/\overline{q}, \quad \text{and} \quad C_T = \tau/R_2 \tag{3.3}$$

with $\overline{p} = 10$ [kPa] the desired mean pressure and $\overline{q}$ the mean flow prescribed at

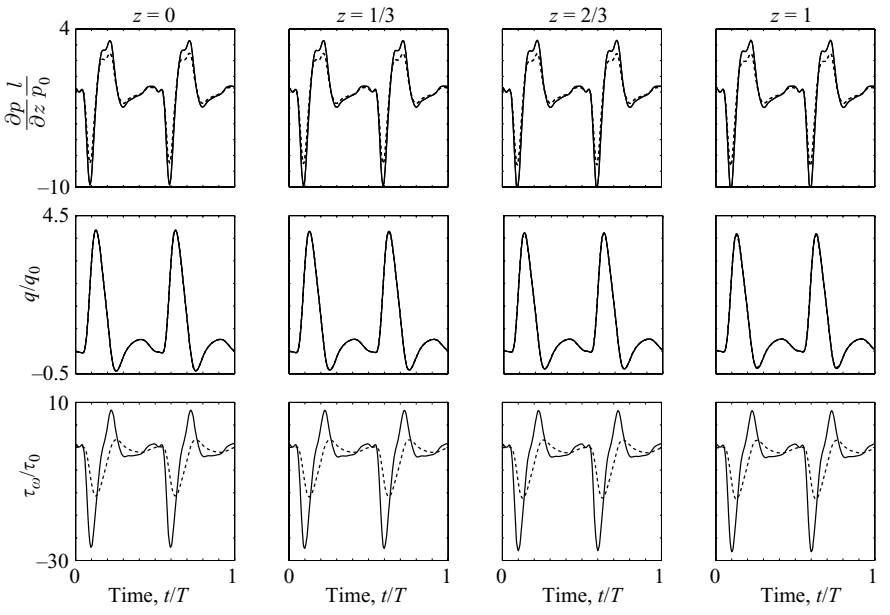

FIGURE 9. As figure 8 but for a femoral-like vessel.

the inlet. By a first-order approximation, the time constant $\tau = 1.5\,\mathrm{s}$ was found to result in a physiological pressure drop in the pressure signal comparable to that demonstrated in the data of Olufsen & Peskin (2000). Note that, similar to the literature, in Poiseuille-friction computations the friction term was altered by replacing the second equation of (2.33) by

$$\tau_w^p = -\frac{a}{2}Rq = -\frac{4\eta}{\pi a^3}q \tag{3.4}$$

and thus changing only the second term on the right-hand side of the momentum equation in (2.32). The volumetric outflow per unit of length was set to $\Psi = 0\ [\mathrm{m^2\,s^{-1}}]$. Since friction is dependent, as well as on flow q, on the pressure gradient $\partial p/\partial z$ and because we are also interested in the wall shear stress τ_w, these two quantities are depicted along with the flow q as a function of time at four equidistant positions in the aorta-like and femoral-like vessel (figures 8 and 9 respectively). Results are captured in the 9th to 10th period when time-periodic pressure and flow was found. All quantities are normalized by dividing them by the mean (over time) of the Poiseuille friction as defined by (3.4). In the aorta-like vessel the two different velocity profiles yield very distinctive wall shear stresses. Friction as approximated by the Poiseuille profile shows the expected in-phase behaviour with the flow and is much smaller than the friction according to the approximate velocity profile function. Looking at the resulting pressure gradient and flow waves in the aorta, however, the effect of the friction approximation used appears negligible, as expected from inertia-dominated flow. In the femoral artery the wall shear stress based on the approximate velocity profile function is of the same order of magnitude as friction approximated by assuming a Poiseuille profile. As a result of the in-phase behaviour of the Poiseuille wall shear stress with the flow, however, it is different from the wall shear stress calculated in this paper, which is dependent on pressure gradient as well as flow. Since in medium-sized and

smaller arteries friction influences the wave propagation, this also results in differences in the pressure gradient. Hence, a suitable friction model is crucial in predicting the pressure and the flow waves propagating through the arterial system, especially for the medium-sized arteries where Poiseuille friction is not appropriate. The reason why the flow is not influenced by the friction term used can be explained by the fact that the flow pulse, as depicted at $z = 0$, is prescribed as an essential boundary condition.

4. Discussion

The theory proposed in this paper uses the division of fluid inside a vessel lumen into a viscous layer close to the wall connected to an inviscid core to obtain first-order approximations for the friction forces and the nonlinear term in one-dimensional wave propagation in the time domain. The local thickness of the viscous layer is determined as a function of the Womersley parameter α, where the definition of α is based on the first harmonic of the flow signal. The method proposed here yields wall shear stresses and convection forces in good agreement with Womersley's theory for time-dependent flow in rigid tubes when a single-harmonic flow pulse is imposed. In the limiting cases ($\alpha = 0$ and $\alpha \to \infty$) Womersley's theory is exactly reproduced by the approximation proposed in this study. For intermediate values of α, both the wall shear stresses and the convection forces show good agreement with Womersley's theory where the velocity profiles obtained show the expected phase difference between the flow in the viscous layer and the core flow. When comparing velocity profiles, the wall shear stress and the nonlinear term based on the approximate velocity profile function with Womersley's solutions, using a more physiological flow pulse based on measurements in the aorta and coronary artery, results similar to Womersley's theory are obtained. So, even though the estimation of the Womersley parameter α is based on only the first harmonic of the flow signal, good approximations for the thickness of the viscous layer for a multi-harmonic flow signal are still obtained, provided the first harmonic is dominant over the higher frequencies involved and not negligibly small compared to the mean level. Since the estimation of the thickness of the Stokes layer was derived for straight vessels with gradual changes in the cross-section area, more sophisticated analysis will be needed to model geometric discontinuities like stenoses and bifurcations. Theories from Schlichting (1960) and Pedley (1980) as well as three-dimensional computational fluid dynamics results and experimental data could be used to derive proper estimates for the thickness of the viscous layer in these regions.

The effect of the wall shear stress derived from the velocity profile approximation in one-dimensional wave propagation was examined by comparing its results to the one-dimensional theory based on Poiseuille friction in an aorta-like and a femoral-like tapered vessel. From these simulations the conclusion could be drawn that in large, inertia-dominated vessels friction is largely under-estimated by assuming Poiseuille profiles, although the influence of an appropriate friction model on the wave propagation phenomena is insignificant. In smaller vessels, however, the choice of an appropriate friction model is important for obtaining reliable wall shear stresses as well as physiological pressure and flow wave propagation characteristics. This implies that using an explicit method to determine the wall shear stress, i.e. no proper friction approximation in the one-dimensional wave propagation equations, will not yield reliable results.

The spectral element framework used for discretization enables simple connection of tubes by adding continuity of pressure and flow in bifurcations. This, together with

appropriate proximal and distal boundary conditions may lead to the modelling of the total arterial tree, where further improvements may be obtained by introducing an appropriate model to predict the local blood viscosity.

In this work, a constant fluid viscosity was assumed whereas it is known that blood viscosity is dependent on the local shear rate through, for example, the aggregation of erythrocytes present in the plasma. Such behaviour may change local velocity profiles resulting in different wall shear stresses. Furthermore, a visco-elasticity model may be incorporated to model the arterial wall behaviour, giving the model more physiological characteristics. This may be achieved by, instead of substituting the constitutive equation into the mass balance, explicitly defining a differential equation describing the wall behaviour (e.g. the standard linear solid model) and building a system of equations with three variables (A, q, p) instead of two (p, q).

Proper evaluation of the model proposed, apart from a comparison to Womersley's theory, could be accomplished by coupling the one-dimensional solutions to a three-dimensional fluid–structure interaction (FSI) model and comparing the predicted wall shear stresses of both theories, or by a comparison of the pressure and flow wave propagation to data sets obtained from experiments.

The model proposed may be used to simulate pressure and flow wave propagation in the time domain to determine the effect of a local arterial pathology on the total arterial system. Bypass surgery alternatives may be evaluated and, combining the pressure and wall shear stress data obtained from this work with a suitable adaptation law for the arterial wall, remodelling of the total arterial system may be studied. As the centreline velocity, corresponding to v_c in the model proposed, can be assessed *in-vivo* by ultrasound systems (Brands *et al.* 1996), this model can also serve as a first-order method to derive the wall shear stress from ultra-sound measurements as an alternative to extrapolation of velocity profiles.

5. Conclusion

A wave propagation model in the time domain is developed where assumptions concerning the velocity profiles are based on a newly developed velocity profile function, dependent not only on the main velocity, but also on the pressure gradient. Using this method, a phase difference between the wall shear stress and the mean velocity similar to that found in physiological situations and by Womersley's theory in the frequency domain is obtained. Also, the approximation of the nonlinear term based on the approximate velocity profile function shows good agreement with Womersley's theory. Implications of the friction term for one-dimensional wave propagation characteristics are illustrated and shown to be significant.

Parts of this research were performed in the scope of the Hemodyn project, which is a cooperation between: Philips Medical Systems (Medical IT Advanced Development), Best, The Netherlands; Eindhoven University of Technology (Biomedical Engineering Department), The Netherlands; Erasmus University (Thoraxcenter, Biomedical Engineering), Rotterdam, The Netherlands. The Hemodyn project is partly funded by SenterNovem (Dutch Ministry of Economic Affairs) in their TS stimulation program.

D.B. is very grateful to Ellen Dudley for the textual correction of this paper.

F. v. d. V. wishes to thank T. J. R. Hughes and C. A. Taylor for their valuable discussions during the first stage of development of this study.

Appendix A. Derivation of the nonlinear part

The derivation of $\gamma(p,q) = A\overline{v_z^2}$ is illustrated by determining the square of the velocity profile $v_z(p,q)$ and integrating the result over cross-sectional area A. The velocity profile as presented in (2.18) is taken as the point of departure:

$$v_z = \frac{-\ln\hat{\zeta}}{1-\zeta_c}\,\overline{v}_z - \frac{a^2}{4\eta}\left[1-\hat{\zeta}+\tfrac{1}{2}(\zeta_c+1)\ln\hat{\zeta}\right]\frac{\partial p}{\partial z} \tag{A 1}$$

or

$$v_z = \phi_1\,\overline{v}_z + \phi_2\,v_p \tag{A 2}$$

with ϕ_1 and ϕ_2 defined as

$$\phi_1 = \frac{-\ln\hat{\zeta}}{1-\zeta_c} \quad \text{and} \quad \phi_2 = 1-\hat{\zeta}+\tfrac{1}{2}(\zeta_c+1)\ln\hat{\zeta} \tag{A 3}$$

and

$$v_p = -\frac{a^2}{4\eta}\frac{\partial p}{\partial z}. \tag{A 4}$$

From this, v_z^2 is given by

$$v_z^2 = \phi_1^2\,\overline{v}_z^2 + 2\phi_1\phi_2\,\overline{v}_z v_p + \phi_2^2\,v_p^2. \tag{A 5}$$

Taking the mean of this term and multiplying by A results in

$$A\overline{v_z^2} = 2\pi\left(\int_0^a \phi_1^2 r\,\mathrm{d}r\right)\overline{v}_z^2 + 2\pi\left(\int_0^a 2\phi_1\phi_2 r\,\mathrm{d}r\right)\overline{v}_z v_p + 2\pi\left(\int_0^a \phi_2^2 r\,\mathrm{d}r\right)v_p^2 \tag{A 6}$$

or, choosing a more appropriate notation and using $\overline{v}_z \equiv q/A$,

$$A\overline{v_z^2} = \int_0^1 \phi_1^2\,\mathrm{d}\zeta\;\frac{q^2}{A} - \int_0^1 2\phi_1\phi_2\,\mathrm{d}\zeta\;q\,v_p + A\int_0^1 \phi_2^2\,\mathrm{d}\zeta\;v_p^2. \tag{A 7}$$

Introducing functions δ_1, δ_2 and δ_3 according to

$$\delta_1(\zeta_c) = \int_0^1 \phi_1^2\,\mathrm{d}\zeta = \frac{2-2\zeta_c(1-\ln\zeta_c)}{(1-\zeta_c)^2}, \tag{A 8a}$$

$$\delta_2(\zeta_c) = -2\int_0^1 \phi_1\phi_2\,\mathrm{d}\zeta = \frac{1+4\zeta_c(1+\ln\zeta_c)-\zeta_c^2(5-2\ln\zeta_c)}{1-\zeta_c}, \tag{A 8b}$$

$$\delta_3(\zeta_c) = \int_0^1 \phi_2^2\,\mathrm{d}\zeta = \tfrac{1}{3}+\zeta_c(3+2\ln\zeta_c)-\zeta_c^2(3-2\ln\zeta_c)-\tfrac{1}{3}\zeta_c^3, \tag{A 8c}$$

yields the expression for $\gamma(p,q)$:

$$\gamma(p,q) = \delta_1\frac{q^2}{A} + \delta_2 q\frac{a^2}{4\eta}\frac{\partial p}{\partial z} + \delta_3 A\left(\frac{a^2}{4\eta}\frac{\partial p}{\partial z}\right)^2. \tag{A 9}$$

Appendix B. Spatial discretization

Strong form

Consider spatial domain $\Omega = [\Gamma_{in}, \Gamma_{out}] \subset \mathbb{R}$ and a time period $T = [0, T_e]$. Assume that $\boldsymbol{N}(\boldsymbol{u}, z, t)$, $\boldsymbol{D}(\boldsymbol{u}, z, t)$, $\boldsymbol{H}(\boldsymbol{u}, z, t)$ and $\boldsymbol{f}(\boldsymbol{u}, z, t)$ are matrices of known functions from $\Omega \to \mathbb{R}$. The strong form of the one-dimensional wave propagation problem is then given by:

Find $\boldsymbol{u}(z,t) = [u_1(z,t), u_2(z,t)] : \Omega \times T \to \mathbb{R} \times \mathbb{R}$ that is a solution of:

$$\left.\begin{array}{ll} \dfrac{\partial \boldsymbol{u}}{\partial t} + \boldsymbol{N}\dfrac{\partial \boldsymbol{u}}{\partial z} - \boldsymbol{D}\dfrac{\partial^2 \boldsymbol{u}}{\partial z^2} + \boldsymbol{H}\boldsymbol{u} = \boldsymbol{f} & \text{in } \Omega, \\ u_2(z,t) = u_{2in}(t) & \text{for } z = \Gamma_{in}, \\ u_1(z,t) = u_{1out}(t) & \text{for } z = \Gamma_{out}, \\ \boldsymbol{u}(z,0) = \boldsymbol{u}^0(z) & \text{for } t = 0, \end{array}\right\} \tag{B 1}$$

with $u_1 = p$ the pressure and $u_2 = q$ the flow. Functions u_{2in} and u_{1out} define the boundary conditions and $\boldsymbol{u}^0(z) = (u_1^0(z), u_2^0(z))$ is a given function that defines the initial condition.

Weak form

To derive a weak form of the problem (B 1) we define the space of trial functions that satisfy the Dirichlet boundary conditions at Γ_{in} and Γ_{out}:

$$\boldsymbol{U} = \{\boldsymbol{u} | \boldsymbol{u} \in H^1(\Omega) \times H^1(\Omega),\ u_1|_{\Gamma_{out}} = u_{1out},\ u_2|_{\Gamma_{in}} = u_{2in}\}. \tag{B 2}$$

Moreover, we define a set of test functions that satisfy the homogeneous Dirichlet conditions:

$$\boldsymbol{W} = \{\boldsymbol{w} | \boldsymbol{w} \in H^1(\Omega) \times H^1(\Omega),\ w_1|_{\Gamma_{out}} = 0,\ w_2|_{\Gamma_{in}} = 0\}. \tag{B 3}$$

Here $H^1(\Omega)$ is the Hilbert space defined by

$$H^1(\Omega) = \left\{ v \in L^2(\Omega) | \int_\Omega \left(\frac{\partial v}{\partial z}\right)^2 \mathrm{d}\Omega < \infty \right\} \tag{B 4}$$

with $L^2(\Omega)$ the space of square integrable functions:

$$L^2(\Omega) = \{v | \int_\Omega v^2 \,\mathrm{d}\Omega < \infty\} \tag{B 5}$$

endowed with the inner product:

$$(u, w)_{L^2} = \int_\Omega u w \,\mathrm{d}\Omega. \tag{B 6}$$

The corresponding weak form of (B 1) is:

Find $\boldsymbol{u}(z,t) \in \boldsymbol{U}$ such that $\forall \boldsymbol{w} \in \boldsymbol{W}$:

$$\int_\Omega w_l \frac{\partial u_l}{\partial t}\,\mathrm{d}\Omega + \sum_{k=1}^{2} \int_\Omega w_l N_{lk} \frac{\partial u_k}{\partial z}\,\mathrm{d}\Omega + \int_\Omega \frac{\partial w_l}{\partial z} D_{lk} \frac{\partial u_k}{\partial z}\,\mathrm{d}\Omega + \int_\Omega w_l H_{lk} u_k \,\mathrm{d}\Omega = \int_\Omega w_l f_l \,\mathrm{d}\Omega \quad \text{for } l = 1,\ 2 \tag{B 7}$$

with N_{lk}, D_{lk}, H_{lk} and f_l the matrix components of matrices $\boldsymbol{N}$, $\boldsymbol{D}$, $\boldsymbol{H}$ and $\boldsymbol{f}$, as defined in (2.43) and (2.44), respectively. Note that the boundary integral resulting from the partial integration of diffusion term $\boldsymbol{D}$

$$\int_\Gamma \boldsymbol{w} \cdot \boldsymbol{D} \frac{\partial \boldsymbol{u}}{\partial z} \mathrm{d}\Gamma = -w_2 D_{22} \frac{\partial u_2}{\partial z}\bigg|_{\Gamma_{out}} \tag{B 8}$$

has been omitted. Since this term $\boldsymbol{D}$-term is small and is only kept for numerical stability, this will not induce strong constraints u_1 and u_2.

Discrete form

With the aid of the basis functions $\phi_i(z)$ we define the subspaces $\boldsymbol{U}^h \subset \boldsymbol{U}$ and $\boldsymbol{W}^h \subset \boldsymbol{W}$ according to

$$\boldsymbol{U}^h = \{\boldsymbol{u}^h | \boldsymbol{u}^h(z,t) = \sum_{i=1}^{N} \boldsymbol{u}_i(t)\phi_i(z),\ u_1^h|_{\Gamma_{out}} = u_{1_{out}},\ u_2^h|_{\Gamma_{in}} = u_{2_{in}}\}, \tag{B 9}$$

$$\boldsymbol{W}^h = \{\boldsymbol{w}^h | \boldsymbol{w}^h(z) = \sum_{i=1}^{N} \boldsymbol{w}_i\phi_i(z),\ w_1^h|_{\Gamma_{out}} = 0,\ w_2^h|_{\Gamma_{in}} = 0\}, \tag{B 10}$$

so after introduction of

$$\underset{\sim}{v}^T = [v_1, \ldots, v_N] \quad \text{for } v = u_1,\ u_2,\ w,\ f,\ \phi \tag{B 11}$$

and using translations

$$\sum_{i=1}^{N} \boldsymbol{u}_i(t)\phi_i(z) = \underset{\sim}{\boldsymbol{u}}^T \cdot \underset{\sim}{\phi} \quad \text{and} \quad \sum_{i=1}^{N} \boldsymbol{w}_i(t)\phi_i(z) = \underset{\sim}{\boldsymbol{w}}^T \cdot \underset{\sim}{\phi}, \tag{B 12}$$

the Galerkin weak form of (B 1) is:

Find $\boldsymbol{u}^h(z,t) \in \boldsymbol{U}^h$ such that $\forall \boldsymbol{w}^h \in \boldsymbol{W}^h$:

$$\begin{aligned}\int_\Omega \underset{\sim}{w_l}^T \underset{\sim}{\phi} \cdot \underset{\sim}{\dot{u}_l}^T \underset{\sim}{\phi}\ \mathrm{d}\Omega\ &+ \sum_{k=1}^{2} \int_\Omega \underset{\sim}{w_l}^T \underset{\sim}{\phi} \cdot N_{lk} \underset{\sim}{u_k}^T \frac{\partial \underset{\sim}{\phi}}{\partial z}\ \mathrm{d}\Omega\ + \int_\Omega \underset{\sim}{w_l}^T \frac{\partial \underset{\sim}{\phi}}{\partial z} \cdot D_{lk} \underset{\sim}{u_k}^T \frac{\partial \underset{\sim}{\phi}}{\partial z}\ \mathrm{d}\Omega \\ &+ \int_\Omega \underset{\sim}{w_l}^T \underset{\sim}{\phi} \cdot H_{lk} \underset{\sim}{u_k}^T \underset{\sim}{\phi}\ \mathrm{d}\Omega = \int_\Omega \underset{\sim}{f_l}^T \underset{\sim}{\phi} \cdot \underset{\sim}{w_l}^T \underset{\sim}{\phi}\ \mathrm{d}\Omega \quad \text{for } l = 1,\ 2\end{aligned} \tag{B 13}$$

or, considering that these equations must hold for all admissible $\underset{\sim}{w} \in \boldsymbol{W}^h$:

Find $\boldsymbol{u}^h(z,t) \in \boldsymbol{U}^h$ such that $\forall \boldsymbol{w}^h \in \boldsymbol{W}^h$:

$$\begin{aligned}\int_\Omega \underset{\sim}{\phi}\underset{\sim}{\phi}^T\ \mathrm{d}\Omega\ \underset{\sim}{\dot{u}_l} &+ \sum_{k=1}^{2} \int_\Omega \underset{\sim}{\phi} N_{lk} \frac{\partial \underset{\sim}{\phi}^T}{\partial z}\ \mathrm{d}\Omega\ \underset{\sim}{u_k} + \int_\Omega \frac{\partial \underset{\sim}{\phi}}{\partial z} D_{lk} \frac{\partial \underset{\sim}{\phi}^T}{\partial z} \mathrm{d}\Omega\ \underset{\sim}{u_k} \\ &+ \int_\Omega \underset{\sim}{\phi} H_{lk} \underset{\sim}{\phi}^T \mathrm{d}\Omega\ \underset{\sim}{u_k} = \int_\Omega \underset{\sim}{\phi}\underset{\sim}{\phi}^T \mathrm{d}\Omega\ \underset{\sim}{f_l} \quad \text{for } l = 1,\ 2,\end{aligned} \tag{B 14}$$

With the introduction of the matrices:

$$\left.\begin{aligned} \underline{M} &= \int_\Omega \underset{\sim}{\phi}\underset{\sim}{\phi}^T \mathrm{d}\Omega, & \underline{N}_{lk} &= \int_\Omega \underset{\sim}{\phi} N_{lk} \frac{\partial \underset{\sim}{\phi}^T}{\partial z} \mathrm{d}\Omega, \\ \underline{D}_{lk} &= \int_\Omega \frac{\partial \underset{\sim}{\phi}}{\partial z} D_{lk} \frac{\partial \underset{\sim}{\phi}^T}{\partial z} \mathrm{d}\Omega, & \underline{H}_{lk} &= \int_\Omega \underset{\sim}{\phi} H_{lk} \underset{\sim}{\phi}^T \mathrm{d}\Omega, \end{aligned}\right\} \tag{B 15}$$

this yields

$$\underline{M}\,\underset{\sim}{\dot{u}_l} + \sum_{k=1}^{2} \underline{N}_{lk}\underset{\sim}{u_k} + \underline{D}_{lk}\underset{\sim}{u_k} + \underline{H}_{lk}\underset{\sim}{u_k} = \underline{M}\,\underset{\sim}{f_l} \quad \text{for } l = 1,\ 2. \tag{B 16}$$

Spectral element approximation

First the basis functions ϕ are restricted to functions that satisfy

$$\phi_i(z_j) = \delta_{ij}, \qquad i = 1, \ldots, N, \tag{B 17}$$

with δ_{ij} the Kronecker delta function and z_j a set of collocation points such that $\Gamma_{in} \leqslant z_j \leqslant \Gamma_{out}$ for $j = 1, \ldots, N$. Consequently the values of the parameters $\boldsymbol{u}_i$ are equal to the approximate solution at the collocation point:

$$\boldsymbol{u}_l^h(z_j) = \sum_{i=1}^{N} \boldsymbol{u}_{l,i}\phi_i(z_j) = \boldsymbol{u}_{l,j}, \qquad j = 1, \ldots, N. \tag{B 18}$$

Secondly the domain Ω is decomposed into a finite number N_e of subdomains (elements) Ω_e. The integrations that appear in (B 15) then can be carried out element by element according to

$$\int_{\Omega} f \,\mathrm{d}\Omega = \sum_{e=1}^{N_e} \int_{\Omega_e} f_e \,\mathrm{d}\Omega \tag{B 19}$$

where f_e is the restriction of f on Ω_e. If we choose the element boundaries to coincide with a subset of the collocation points, to satisfy (B 17), we can define the basis functions by the Lagrange interpolation polynomials through the $n + 1$ collocation points in each element:

$$\phi_i(z) = \frac{\displaystyle\prod_{k=0,k\neq i}^{n} (z - z_k)}{\displaystyle\prod_{k=0,k\neq i}^{n} (z_i - z_k)}, \qquad i = 0, \ldots, n. \tag{B 20}$$

Finally we use a Legendre–Gauss–Lobatto integration and choose the Lagrange interpolation points to be equal to the Legendre–Gauss–Lobatto points:

$$\int_{\Omega_e} f(z) \,\mathrm{d}z = \int_{-1}^{1} f(\xi) \frac{dz}{\mathrm{d}\xi} \mathrm{d}\xi \approx \sum_{k=0}^{n} f\left(\xi_k^{gl}\right) J\left(\xi_k^{gl}\right) w_k^{gl} \tag{B 21}$$

with ξ_k^{gl} the Legendre–Gauss–Lobatto integration points defined as the zeros of the first derivative of the nth-order Legendre polynomial $L_n(\xi)$ extended with the element boundary $\xi_0 = -1$, $\xi_n = 1$, $J(\xi_k^{gl})$ the Jacobian $\mathrm{d}z/\mathrm{d}\xi$, and w_k^{gl} the Legendre–Gauss–Lobatto weight functions defined by Canuto *et al.* (1988):

$$w_k^{gl} = \frac{2}{n(n+1)} \frac{1}{L_n^2(\xi_k)}, \qquad k = 0, \ldots, n. \tag{B 22}$$

REFERENCES

Anliker, M., Rockwell, L. & Ogden, E. 1971 Nonlinear analysis of flow pulses and shock waves in arteries. *Z. Angew. Math. Phys.* **22**, 217–246.

Brands, P. J., Hoeks, A. P. G., Rutten, M. C. M. & Reneman, R. S. 1996 A non-invasive method to estimate arterial impedance by means of the assessment of the local diameter change and the local centre-line blood flow velocity using ultrasound. *Ultrasound Med. Biol* **7**, 895–905.

Canuto, C., Hussaini, M. Y., Quarteroni, A. & Zang, T. A. 1988 *Spectral Methods in Fluid Dynamics*. Springer.

Cox, R. H. 1968 Wave propagation through a newtonian fluid contained within a thick-walled viscoelastic tube. *Biophys. J.* **8**, 691–709.

Cox, R. H. 1970 Wave propagation through a newtonian fluid contained within a thick-walled viscoelastic tube: the influence of wall compressibility. *J. Biomech.* **3**, 317–335.

Formaggia, L., Gerbeau, J. F., Nobile, F. & Quarteroni, A. 2001 On the coupling of 3d and 1d navier-stokes equations for flow problems in compliant vessels. *Comput. Methods Appl. Mech. Engng* **191**, 561–582.

Fung, Y. C. 1993 *Biomechanics: Mechanical Properties of Living Tissues.* Springer.

Gijsen, F. J. H., van de Vosse, F. N. & Janssen, J. D. 1999*a* Influence of the non-newtonian properties of blood on the flow in large arteries: Steady flow in a carotid bifurcation model. *J. Biomech.* **32**, 601–608.

Gijsen, F. J. H., van de Vosse, F. N. & Janssen, J. D. 1999*b* Influence of the non-newtonian properties of blood on the flow in large arteries: Unsteady flow in a 90-degree curved tube. *J. Biomech.* **32**, 705–713.

Hughes, T. J. R. & Lubliner, J. 1973 On the one-dimensional theory of blood flow in the large vessels. *Math. Bioscie.* **18**, 161–170.

Lagrée, P.-Y. 2000 An inverse technique to deduce the elasticity of a large artery. *Euro. Phys. J. AP* **9**, 153–163.

Olufsen, M. S. 1999 Structured tree outflow condition for blood flow in larger systemic arteries. *Am. J. Physiol.* **276**, H257–H268.

Olufsen, M. S. & Peskin, C. S. 2000 Numerical simulation and experimental validation of blood flow in arteries with structured-tree outflow conditions. *Ann. Biomed. Engng* **28**, 1281–1299.

de Pater, L. & van den Berg, J. W. 1964 An electrical analogue of the entire human circulatory system. *Med. Electron. Biol. Engng* **2**, 161–166.

Pedley, T. J. 1980 *The Fluid Mechanics of Large Blood Vessels.* Cambridge University Press.

Porenta, G., Young, D. F. & Rogge, T. R. 1986 A finite element model of blood flow in arteries including taper, branches and obstructions. *J. Bio. Engng* **108**, 161–167.

Schlichting, H. 1960 *Boundary Layer Theory.* McGraw-Hill.

Sherwin, S. J., Formaggia, L., Peiró, J. & Franke, V. 2003 Computational modelling of 1d blood flow with variable mechanical properties and its application to the simulation of wave propagation in the human arterial system. *Intl J. Num. Meth. Fluids* **43**, 673–700.

Stergiopulos, N., Westerhof, B. E. & Westerhof, N. 1999 Total arterial inertance as the fourth element of the windkessel model. *Am. J. Physiol.* **276**, H81–H88.

Stergiopulos, N., Young, D. F. & Rogge, T. R. 1992 Computer simulation of arterial flow with applications to arterial and aortic stenoses. *J. Biomech.* **25**, 1477–1488.

Taylor, C. A., Hughes, T. J. R. & Zarins, C. K. 1998 Finite element modeling of blood flow in arteries. *Comput. Meth. Appl. Mech. Engng* **158**, 155–196.

Tsou, F. K., Chou, P. C., Frankel, S. N. & Hahn, A. W. 1971 An integral method for the analysis of blood flow. *Bull. Math. Biophys.* **33**, 117–128.

van de Vosse, F. N., de Hart, J., van Oijen, C. H. G. A., Bessems, D., Gunther, T. W. M., Segal, A., Wolters, B. J. B. M., Stijnen, J. M. A. & Baaijens, F. P. T. 2003 Finite-element-based computational methods for cardiovascular fluid-structure interaction. *J. Engng Maths* **47**, 335–368.

Wan, J., Steele, B., Spicer, S. A., Strohband, S., Feijoo, C. R., Hughes, T. J. R. & Taylor, C. A. 2002 A one-dimensional finite element method for simulation-based medical planning for cardiovascular disease. *Computer Meth. Biomech. Biomed. Engng,* pp. 195–206.

Wang, J. J. & Parker, H. H. 2004 Wave propagation in a model of the arterial circulation. *J. Biomech.* **37**, 457–470.

Westerhof, N., Bosman, F., de Vries, Co. J. & Noordergraaf, A. 1969 Analog studies of the human systemic arterial tree. *J. Biomech.* **2**, 121–143.

Womersley, J. R. 1957 An elastic tube theory of pulse transmission and oscillatory flow in mammalian arteries. *Tech. Rep. WADC-TR*-56-614.

Young, D. F. & Tsai, F. Y. 1973 Flow characteristics in models of arterial stenoses-ii. unsteady flow. *J. Biomech.* **6**, 547–559.

Zagzoule, M., Khalid-Naciri, J. & Mauss, J. 1991 Unsteady wall shear stress in a distensible tube. *J. Biomech.* **24**, 435–439.